Statistical Characteristics of Unsteady Storms in Radar Observations for the Beijing–Tianjin Region

YU WANG AND HONG-QING WANG

Department of Atmospheric and Oceanic Sciences, School of Physics, Peking University, Beijing, China

LEI HAN

College of Information Science and Engineering, Ocean University of China, Qingdao, and State Key Laboratory of Severe Weather, Chinese Academy of Meteorological Sciences, Beijing, China

YIN-JING LIN

National Meteorological Center of the China Meteorological Administration, Beijing, China

YAN ZHANG

Department of Atmospheric and Oceanic Sciences, School of Physics, Peking University, Beijing, China

(Manuscript received 11 February 2014, in final form 25 September 2014)

ABSTRACT

This study was designed to provide basic information for the improvement of storm nowcasting. According to the mean direction deviation of storm movement, storms were classified into three types: 1) steady storms (S storms, extrapolated efficiently), 2) unsteady storms (U storms, extrapolated poorly), and 3) transitional storms (T storms). The U storms do not fit the linear extrapolation processes because of their unsteady movements. A 6-yr warm-season radar observation dataset was used to highlight and analyze the differences between U storms and S storms. The analysis included geometric features, dynamic factors, and environmental parameters. The results showed that storms with the following characteristics changed movement direction most easily in the Beijing–Tianjin region: 1) smaller storm area, 2) lower thickness (echo-top height minus base height), 3) lower movement speed, 4) weaker updrafts and the maximum value located in the mid- and upper troposphere, 5) storm-relative vertical wind profiles dominated by directional shear instead of speed shear, 6) lower relative humidity in the mid- and upper troposphere, and 7) higher surface evaporation and ground roughness.

1. Introduction

Nowcasting is a hot issue in the field of mesoscale meteorology. Nowcasting techniques can be divided into three classes (Wilson et al. 1998): 1) extrapolation techniques, 2) numerical prediction techniques, and 3) expert systems with conceptual models. Extrapolation methods based on radar echoes are robust and have better forecast skill than do numerical prediction methods in short-term quantitative precipitation forecasting (Lin et al. 2005; Wilson et al. 2010). Linear or nonlinear extrapolation algorithms can predict storm location, intensity, and scope in the subsequent 0–2 h based on historical observation data. Their forecast skill falls off rapidly with forecast lead time (Golding 1998), especially after 30 min. This is because extrapolation algorithms that only use radar observation data cannot handle storm initiation, growth, and dissipation properly (Browning and Collier 1989; Wilson 2004).

So far, efforts to improve skillful forecasting have mainly focused on improving algorithms (Germann and Zawadzki 2002; Winterrath and Rosenow 2007; Liang et al. 2010; Mandapaka et al. 2012; Radhakrishna et al. 2013; Nisi et al. 2014; Zahraei et al. 2013). Most of these studies only gave improved algorithms and listed the probability of detection, false-alarm ratio, and critical success index scores by them; they have not made

Corresponding author address: Hong-Qing Wang, Dept. of Atmospheric and Oceanic Sciences, School of Physics, Peking University, Beijing 100871, China.
E-mail: hqwang@pku.edu.cn

DOI: 10.1175/JAMC-D-14-0043.1

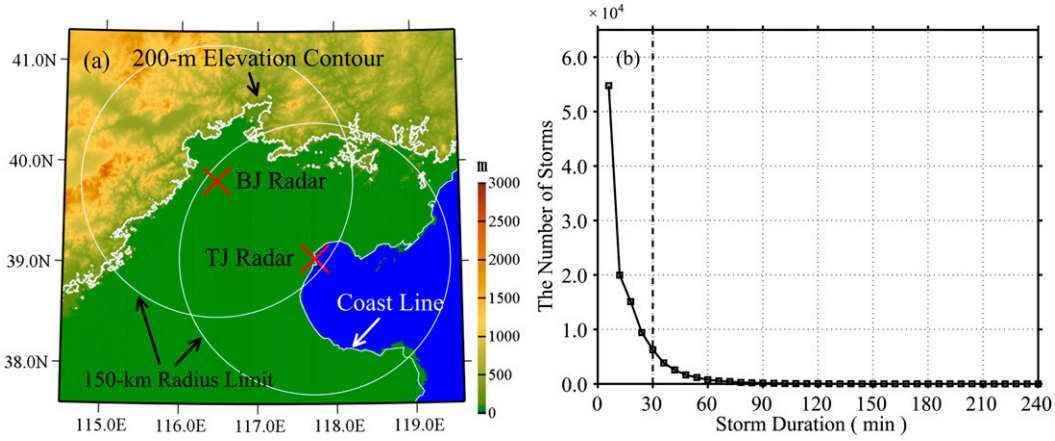

FIG. 1. (a) Terrain around the study area. Colors represent the altitude (m). The red crosses show the positions of the Beijing and Tianjin radar stations. The thick lines indicate the 200-m elevation contour. The circles are the 150-km-radius limit of the radars. (b) Duration distribution of storms identified and tracked by TITAN. The black dashed line in (b) is the 30-min threshold.

a detailed analysis of unsteady storms, which cannot be extrapolated efficiently.

Most current extrapolation methods can effectively predict temporal changes of steady (steady movement) storms. Proper handling of storms that are characterized by rapid temporal changes (unsteady movement) is a key goal for improving forecast skill. A key problem arises from the fact that it is difficult to describe the internal physical structure of storms only using radar data. Hence, other auxiliary data (observation and forecast data) should be used to achieve this goal.

Many factors can affect the temporal and spatial changes of storms, like the storm-scale dynamics and environmental factors. Coniglio et al. (2011, 2012) analyzed the complex environment and early evolution of the 8 May 2009 derecho-producing convective system that occurred in the central United States. Jessup and Colucci (2012) presented the environment conditions of a back-building merging (BBMERGE) event that occurred in the northeastern United States.

This study used the Thunderstorm Identification, Tracking, Analysis, and Nowcasting (TITAN) algorithm (Dixon and Wiener 1993; Han et al. 2009a) to identify and track storms with 6 years of warm-season (May–August 2008–13) radar data. First, the identified storms were classified into three types: 1) steady storms (S storms), 2) unsteady storms (U storms), and 3) transitional storms (T storms). Second, the statistical characteristics of S and U storms were analyzed from the perspective of their geometrical features, dynamic factors, and environmental parameters. This is a basic study for improving forecast quality.

Section 2 introduces the radar and reanalysis data used in this study. Section 3 presents the criteria and practical value of the classification, and then analyzes the diurnal variations of the three storm types. The detailed differences between S and U storms are discussed in section 4. Section 5 presents a summary and discussion of possible future work.

2. Data

a. Radar data and storms

We analyzed 6 years of warm-season (May–August 2008–13) reflectivity data from radar observations of two operational China New Generation Weather Radar System (CINRAD) radars (the Beijing radar station located at 39.81°N, 116.47°E, and the Tianjin radar station at 39.04°N, 117.73°E; Fig. 1a). The temporal resolution was 6 min. A limitation of 150-km radius (Wulfmeyer et al. 2011) was required to achieve the storm analysis. A fuzzy logic algorithm (Kessinger et al. 2003; Liu et al. 2007) was used to remove anomalous propagation (AP) echoes. Most of the AP clusters could be eliminated by this algorithm. Then, the radar observation data were transformed into 3D Cartesian coordinates with a horizontal resolution of 0.01° × 0.01°, a vertical resolution of 1 km, and a temporal resolution of 6 min.

The TITAN algorithm was used to identify and track storms from the 3D grid data. In the storm identification process, we used 35 dBZ as the reflectivity threshold and 30 km^3 as the volume threshold (Han et al. 2009b). A total of 117 449 storms were identified and tracked by the TITAN algorithm. Storms lasting at least 30 min (a total of 18 011 storms) were reserved for subsequent analysis. Figure 1b shows the duration distribution of all 117 449 storms.

b. Terrain and environmental field data

The terrain data were downloaded from the National Geophysical Data Center. Their grid resolution was 30 arc s. In the statistical region, the 200-m contour line marked the boundary between mountains and plains.

The atmospheric environmental field data were provided by the European Centre for Medium-Range Weather Forecasts (ECMWF) interim reanalysis (ERA-Interim; Dee et al. 2011). This dataset contains surface evaporation and ground roughness data at the surface level, the u and v wind field, vertical velocity, relative humidity, and temperature field at 37 levels (from 1000 to 1 hPa). The horizontal and temporal resolutions were $0.75° \times 0.75°$ and 6 h, respectively. For the convective structures that undergo a nonlinear evolution within the 6-h time window, we assumed the ERA-Interim dataset could represent the real atmospheric environment within ±1-h window. This hypothesis indicates when the ERA-Interim dataset was used to calculate vertical velocity, u and v wind field, relative humidity, temperature, surface evaporation, and ground roughness, we only selected storms within ±1 h of the reanalysis time.

3. Method

a. Classification method

Let n denote the number of time steps of a storm (the time step interval is about 6 min in radar observations). Here **vo** denotes the observation (real) motion vector, $\mathbf{vo}_i$ is **vo** at t_i (the ith time step of a storm, $i \in [1, n]$; Fig. 2), **ve** denotes the linear extrapolation motion vector, and $\mathbf{ve}_i = 0.5(\mathbf{ve}_{i-2} + \mathbf{ve}_{i-1})$ is **ve** at t_i.

The mean direction deviation (MDD) of a storm is defined as

$$\mathrm{MDD} = \frac{1}{n-3}\sum_{i=3}^{n-1} \mathrm{abs}[\mathrm{dir}(\mathbf{vo}_i) - \mathrm{dir}(\mathbf{ve}_i)], \qquad (1)$$

where dir() is the direction angle of the vector.

Storms can be classified into three types by MDD: 1) S storms (MDD ≤ 15°), which are extrapolated efficiently; 2) U storms (MDD > 30°), which are extrapolated poorly; and 3) T storms (15° < MDD ≤ 30°), which are used to make the differences between U and S storms more obvious.

Because the purpose of this study was to analyze the differences between S and U storms, T storms were omitted in some cases (‘‘omit’’ means we do not show them in figures and text, but this type always exists).

Taking into account that the spatial resolution of the ERA-Interim dataset did not match that of radar data, storms were divided into small storms and large storms according to the storm’s horizontal scale: 1) large storms: the horizontal scales no less than 20 km, that is, meso-β scale (Orlanski 1975), this includes large S storms (S_L storms) and large U storms (U_L storms); and 2) small storms: the horizontal scales less than 20 km, that is, meso-γ scale (Orlanski 1975), this includes small S storms (S_S storms) and small U storms (U_S storms).

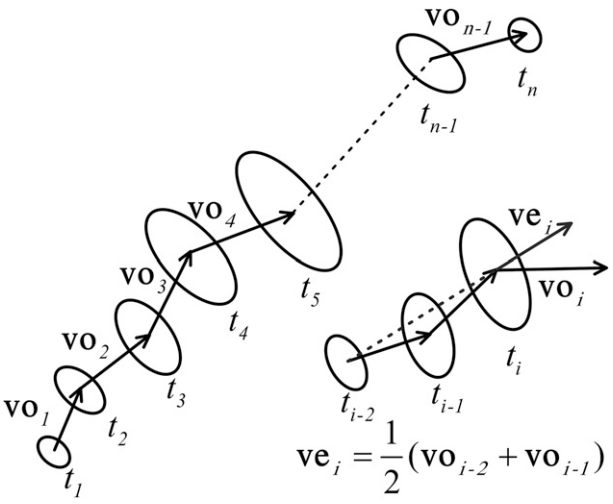

FIG. 2. Schematic of a storm: $\mathbf{vo}_i$ denotes the real motion vector at the ith step of the storm; $\mathbf{ve}_i$ denotes the linear extrapolation vector for the ith step of the storm, and $i \in [1, n]$, n is the number of time steps for a storm.

The subscripts ‘‘S’’ and ‘‘L’’ indicated small and large storms, respectively. For small storms, the ERA-Interim dataset can represent the background field, and for large storms, the ERA-Interim dataset can represent the real atmospheric environment. Then in section 4b (for vertical velocity and horizontal wind field), section 4c (for relative humidity and temperature), and section 4d (for surface evaporation and ground roughness), storms were classified into four groups: S_S storms, U_S storms, S_L storms, and U_L storms.

b. Diurnal distribution

During the 2008–13 warm seasons, 18 011 storms had a duration ≥30 min. According to the classification method (in section 3a), there were 6869 S storms, 6588 U storms, and 4554 T storms within the statistical time range. Figure 3 shows the diurnal distribution of S, U, and T storms, including their quantity (Fig. 3a) and the occurrence ratio (Fig. 3b, only S storms and U storms). The U (S) storms’ occurrence ratio is the number of U (S) storms divided by the number of all storms under certain conditions [e.g., 1300–1400 local standard time (LST)]. The circles in figures indicate the statistical difference passed the significance test, and the crosses indicate the statistical difference did not pass. All significance tests used the one-sided Wilcoxon–Mann–Whitney rank-sum

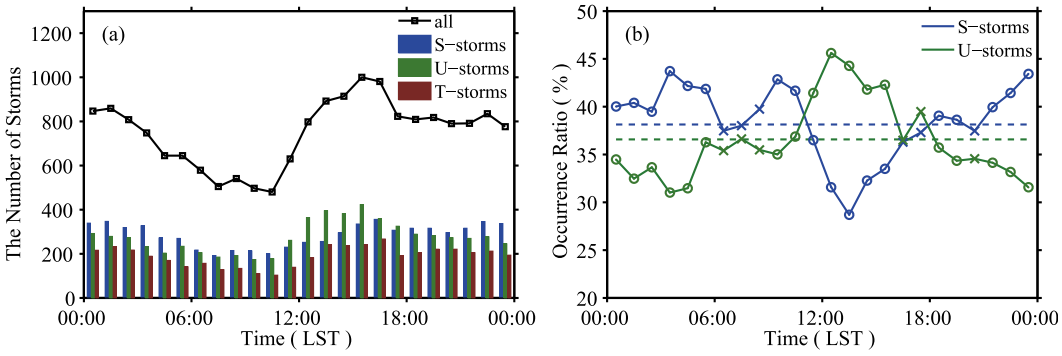

FIG. 3. (a) Quantity and (b) occurrence ratio of storms in a diurnal distribution. In (a), the black line is the total number of storms (including S, U, and T storms), and the blue, dark green, and brown lines show S, U, and T storms. In (b), the dashed lines are the average occurrence ratio. The circles indicate that the difference passed the significance test at the 15% level, and the crosses indicate that the difference did not pass (the same hereinafter).

test as the Lilliefors test showed the parameter distribution did not follow a normal distribution. Except in section 4e, we used 15% as the significance level. In section 4e, the significance levels were 5%, 10%, and 15%.

From the diurnal distribution, the following can be seen. 1) The total number of storms (Fig. 3a) increased after 1100 LST, but the occurrence ratio of S storms decreased (Fig. 3b). 2) The S storms had a high occurrence ratio during the night–morning period (2100–0600 LST), but the ratio began to decline around 1100 LST, reaching a minimum (28.70%) at 1300–1400 LST, and then slowly increasing. 3) In contrast to the S storms, the U storms' occurrence ratio began to increase around 1100 LST and reached a maximum (45.61%) at noon (1200–1300 LST). Increased ratio of the U storms would decrease the general forecast quality.

Generally (in Fig. 3b), U storms were common from 1100 to 1600 LST, whereas S storms were common at other times. The period 1100–1600 LST could be further separated into two stages: 1) 1100–1400 LST: the occurrence ratio of U storms increased rapidly, whereas that of S storms decreased rapidly; and 2) 1400–1600 LST: the occurrence ratio of S storms increased, whereas that of U storms decreased. We supposed the increased occurrence ratio of S storms in stage 2 was due to the steady growth of the storms. For stage 1, a partial explanation related to surface evaporation was shown in section 4d.

c. *Root-mean-square error of U and S storms*

To estimate whether the classification had practical value, we compared the root-mean-square error (RMSE) of U and S storms. We denote the RMSE between **vo** and **ve** as RMSE-e, the RMSE between **vo** and **vp** as RMSE-*p* [where *p* is the pressure level (hPa) from the corresponding ERA-Interim dataset and **vp** is the environment wind vector at pressure level *p*] and the RMSE between **vo** and **vs** as RMSE-s (where **vs** is the 850–300-hPa mean steering flow). Because velocity vectors can be decomposed into two components, speed and direction, the RMSE were also decomposed into two parts. The values are shown in Table 1. Most of the results passed the significance test at the 15% level. The

TABLE 1. The RMSE of U and S storms between **vo** and **vp** (RMSE-*p*, where *p* is from 500 to 850 hPa), the RMSE between **vo** and **ve** (RMSE-e), and the RMSE between **vo** and **vs** (RMSE-s). The boldface numbers indicate the minimum values of RMSE-*p*. The italic numbers indicate that the values do not pass the significance test at the 15% level.

	S storms		U storms	
	Speed ($m\,s^{-1}$)	Direction (°)	Speed ($m\,s^{-1}$)	Direction (°)
RMSE-500	5.55	36.06	6.67	76.67
RMSE-550	5.04	33.76	5.77	75.57
RMSE-600	**4.91**	*31.60*	5.22	*74.40*
RMSE-650	5.07	**30.68**	4.93	**73.78**
RMSE-700	5.48	33.14	**4.87**	73.79
RMSE-750	6.01	39.17	7.99	75.03
RMSE-800	6.63	*49.52*	5.18	*78.97*
RMSE-850	7.36	63.60	5.37	84.90
RMSE-e	3.81	19.38	4.82	76.92
RMSE-s	5.64	36.79	6.61	78.02

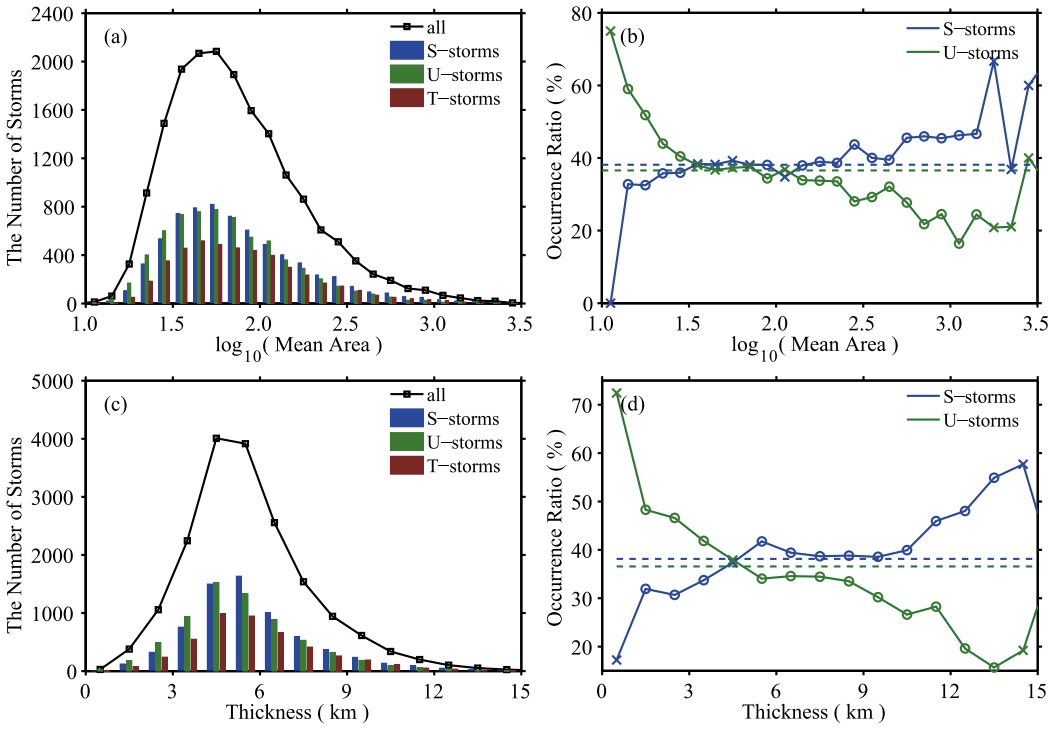

FIG. 4. As in Fig. 3, but for the (a) quantity and (b) occurrence ratio of the storm area (km^2) and the (c) quantity and (d) occurrence ratio of thickness (km).

italic numbers in Table 1 indicated that the results did not pass the significance test at the 15% level.

For S storms, the minimum values of RMSE-*p* were 4.91 $m\,s^{-1}$ (speed) and 30.68° (direction). These were much larger than the minimum values of RMSE-e (3.81 $m\,s^{-1}$ and 19.38°, corresponding to the speed and direction components, respectively). The same situation occurred in the comparison between RMSE-s and RMSE-e. This indicated that using auxiliary data (other observations and forecast data) to guide the motion trend of S storms may cause unexpected errors.

For U storms, the minimum value of RMSE-*p* (73.78°) was smaller than that of RMSE-e (76.92°) and RMSE-s (78.02°) in the direction component. Considering that the spatial resolution of the ERA-Interim dataset is coarse, in the real-time extrapolation operation a higher-spatial-resolution dataset (provided by an NWP model) should be used. As VandenBerg et al. (2014) mentioned, the reduction from 4- to 1-km grid spacing could potentially improve forecasts of storm motion. This indicated that the forecast quality of U storms could be improved by a carefully designed extrapolation method (guided by the auxiliary data).

In the next section, we describe how a smaller storm area, lower thickness, slower movement speed, weaker updraft, directionally sheared storm-relative wind profile, larger surface evaporation and ground roughness, and higher relative humidity at low levels are conducive to the emergence of U storms.

4. Statistical characteristics

a. *Geometric features*

For any storm, geometric features provided by the radar observation data include echo-top height, thickness (echo-top height minus echo-base height), area, and volume. Here, we only consider the effect of storm area and thickness on storm movement steadiness. Because the storm area and thickness change over time, we used the mean area and thickness as statistical parameters. Here, the mean value refers to all time steps in the storm-life history.

Figures 4a and 4b show the area distribution of S, U, and T storms, as well as their quantity (Fig. 4a) and the occurrence ratio (Fig. 4b, only for S and U storms). The unit of area is kilometers squared, and $\log_{10}$(mean area) was used as the *x* axis. As shown in Fig. 4b, where the mean area was lower than 31.6 ($\sim 10^{1.5}$) km^2, U storms had a higher occurrence ratio than did S storms. If the mean area was higher than 125.9 ($\sim 10^{2.1}$) km^2, S storms had a higher occurrence ratio. When the mean area was between 31.6 and 125.9 km^2, the occurrence ratio's difference between U and S storms was not significant. If

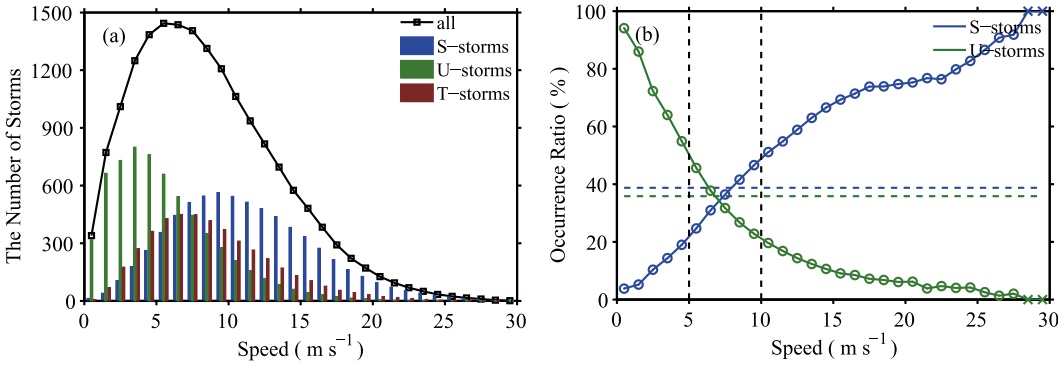

FIG. 5. As in Fig. 3, but for the (a) quantity and (b) occurrence ratio of the mean movement speed (m s^{-1}). The black dashed lines in (b) represent the 5 and 10 m s^{-1} thresholds.

the mean area of a storm was too large or small (e.g., the area was larger than 1500 km^2), the number of samples is too small to calculate the occurrence ratio. Therefore the result could not pass the significance test.

Figures 4c and 4d are the same as Figs. 4a and 4b, but for the thickness distribution. The U storms had a higher occurrence ratio when the mean thickness was less than 4 km. In general, the occurrence ratio of S storms increased with thickness, whereas that of U storms decreased. The storm area and thickness hence directly correlated to movement steadiness; if a storm had a smaller area and lower thickness, the storm was more likely to be a U storm. In particular, when the thickness was less than 4 km, the chance of a U storm was much higher.

b. *Dynamic factors*

Dynamic factors have important influences on the steadiness of storm movement, including on the storm movement speed, the environmental vertical velocity, and the environmental wind field. Figure 5 shows the distribution of mean speed of storm movement, including the quantity (Fig. 5a) and the occurrence ratio (Fig. 5b, only S and U storms). S storms became more frequent as their speed increased. For U storms, the trend was opposite. For example, when the speed was lower than 5 m s^{-1}, a total of 72.28% of storms were U storms. When the speed was higher than 10 m s^{-1}, only 11.94% of storms were U storms. Therefore, U storms and S storms had obvious differences in movement speed.

The mean vertical velocity (MVV) and wind profiles of U and S storms are shown in Fig. 6. For a storm, its vertical velocity (VV) is defined as

$$\mathrm{VV} = \frac{1}{n}\sum_{i=1}^{n} \mathrm{vv}_i, \tag{2}$$

where vv_i is the storm's vertical velocity at t_i. For all storms, the range of VV is [$\mathrm{VV}_{\min}$, $\mathrm{VV}_{\max}$]. The upper quartile value of VV is VV_{q1}; the lower quartile value is VV_{q3}. Therefore the valid range of VV is [$\mathrm{VV}_{\mathrm{lower}}$, $\mathrm{VV}_{\mathrm{upper}}$], where

$$\mathrm{VV}_{\mathrm{upper}} = \min[\mathrm{VV}_{\max}, \mathrm{VV}_{q1} + 1.5(\mathrm{VV}_{q1} - \mathrm{VV}_{q3})] \quad \text{and} \tag{3}$$

$$\mathrm{VV}_{\mathrm{lower}} = \max[\mathrm{VV}_{\min}, \mathrm{VV}_{q3} - 1.5(\mathrm{VV}_{q1} - \mathrm{VV}_{q3})]. \tag{4}$$

Because the box-and-whiskers plot has a higher tolerance in the recognition of outliers of nonnormal distribution data, $\mathrm{VV}_{\mathrm{lower}}$ and $\mathrm{VV}_{\mathrm{upper}}$ were used as the threshold of outliers in this research. Thus the MVV is defined as

$$\mathrm{MVV} = \frac{1}{m}\sum_{\mathrm{VV}\in[\mathrm{VV}_{\mathrm{lower}},\mathrm{VV}_{\mathrm{upper}}]} \mathrm{VV}, \tag{5}$$

where m is the number of storms that satisfied the condition VV $\in$ [$\mathrm{VV}_{\mathrm{lower}}$, $\mathrm{VV}_{\mathrm{upper}}$]. The same method was used in calculating mean wind speed (u and v components, in section 4b), mean temperature and mean relative humidity (in section 4c). The statistical differences of MVV profiles between $\mathrm{S_S}$ and $\mathrm{U_S}$ storms and between $\mathrm{S_L}$ and $\mathrm{U_L}$ storms are discussed below (i.e., only test the statistical significance between two types of small storms, and two types of large storms). The dMVV and MVV have the same calculation method but replaced VV by dVV in Eqs. (2)–(5). The dVV is defined as

$$\mathrm{dVV} = \frac{1}{n-1}\sum_{i=1}^{n-1} \frac{(\mathrm{vv}_{i+1} - \mathrm{vv}_i)}{\mathrm{dis}_{i,i+1}}, \tag{6}$$

where $\mathrm{dis}_{i,i+1}$ is the distance between the storm's ith and $i+1$st centroid position in meters.

Four groups of storms' MVV profiles are shown in Fig. 6a. When compared with U storms, S storms' MVV

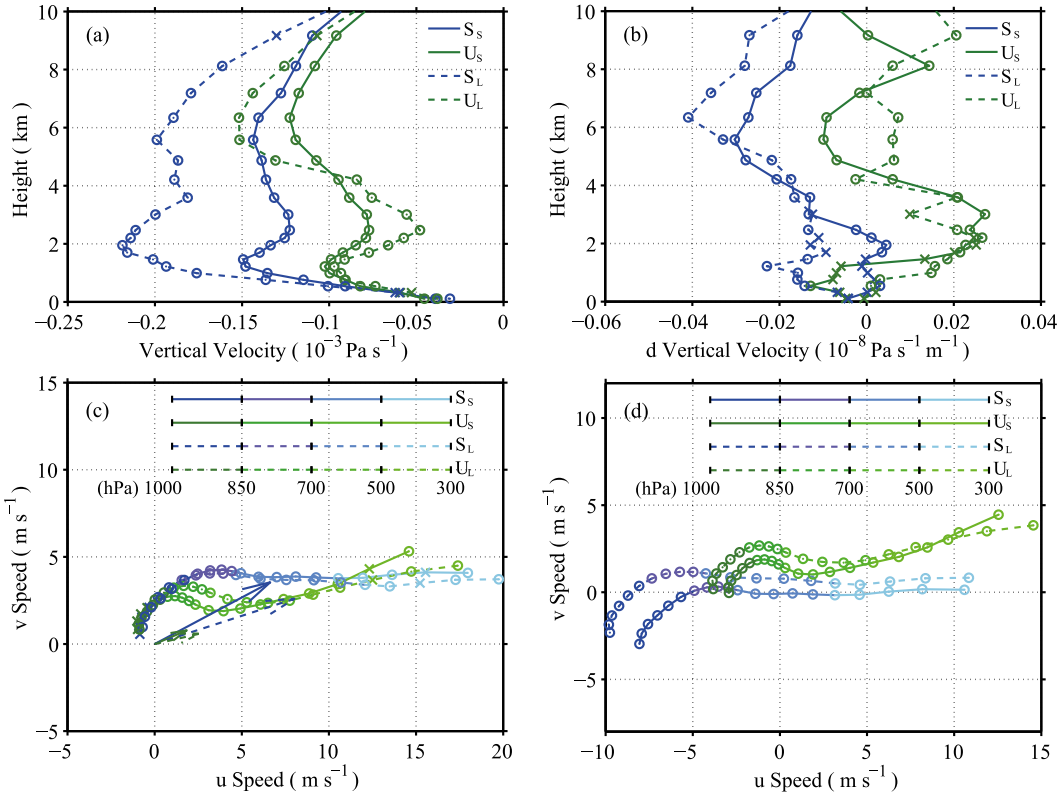

FIG. 6. (a) MVV (Pa s^{-1}) profile, (b) dMVV (Pa s^{-1} m^{-1}) profile, (c) mean wind (m s^{-1}) profile, and (d) mean storm-relative wind (m s^{-1}) profile of U and S storms in the context of u vs v. The vector in (c) is the mean motion vector of the storms. The gradient direction is along the storm trajectory. Here, S_S is small S storms, U_S is small U storms, S_L is large S storms, and U_L is large U storms.

was large (the absolute value) and negative at 925–600 hPa, indicating S storms had a stronger updraft than U storms in the lower and midtroposphere. The maximum value of S storms' MVV profile appeared in the lower troposphere (800 hPa for S_L storms and 850 hPa for S_S storms). In contrast, the maximum value of U storms' MVV profile appeared at the 450-hPa level. Figure 6b is the MVV gradient (dMVV) profiles (the gradient direction is along the storm trajectory, the same hereinafter). In general, the S storms' dMVV had a negative value and the U storms' dMVV had a positive value. This indicated that the large storms' updraft or small storms' background updraft tended to increase (decrease) along S (U) storms trajectory, respectively. Therefore if the updraft or the background updraft was relatively weak and showed a decreasing trend, meanwhile the maximum value located in the mid- and upper troposphere, the storm had a high chance of being a U storm.

Figure 6c shows the mean wind profiles of U and S storms in the context of u versus v. Most of the mean wind profiles passed the significance test, except large storms' wind profiles below the 925-hPa level. The wind profiles showed no significant difference at low levels (850 hPa and below). Above the 850-hPa level, however, the wind profile of U storms showed strong directional shear. Meanwhile, that of the S storms showed strong speed shear. This phenomenon was clearer for the storm-relative wind profiles (Markowski and Richardson 2006) in Fig. 6d: if a storm-relative wind profile (corresponding to large storms) or a background storm-relative wind profile (corresponding to small storms) was dominated by a directional shear, the storm had a higher chance of being a U storm.

c. *Temperature and relative humidity*

In principle, both temperature and relative humidity could affect storm steadiness. However, the statistical results showed no obvious effect of temperature on steadiness. The statistical differences between U and S storm mean relative humidity (MRH) and mean temperature (MT) are shown in Fig. 7.

Figure 7a shows the MRH profile of U and S storms. Small storms' MRH had significant difference above the 775-hPa level, and for large storms the difference was significant above 600 hPa. The S storms' MRH was larger than that of U storms. Figure 7b is the MRH

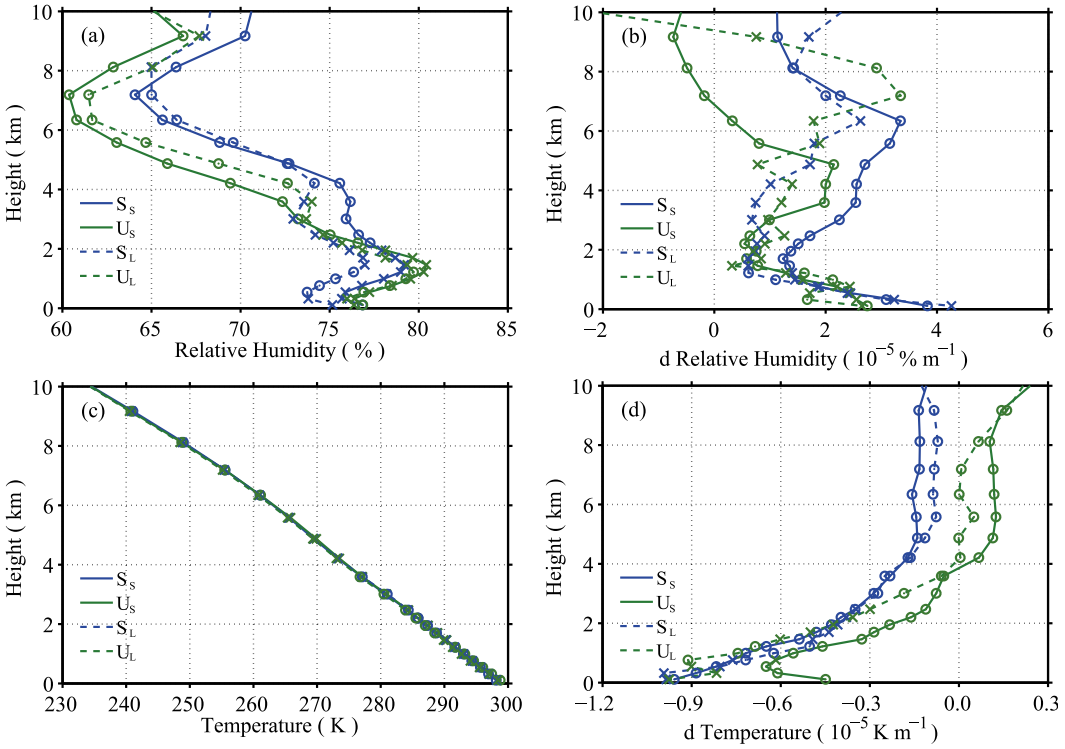

FIG. 7. As in Figs. 6a,b, but for the (a) MRH (%) profile, (b) dMRH (% m^{-1}) profile, (c) MT (K) profile, and (d) dMT (K m^{-1}) profile of U and S storms.

gradient (dMRH) profile. For large storms' dMRH profile, most of the values did not pass the significance test. Therefore the dMRH of large storms did not show significant difference. S_S storms' dMRH was larger than that of U_S storms especially above the 550-hPa level (4.87 km).

Figure 7c shows the MT profile for U and S storms. No significant difference between the profiles was observed. Figure 7d shows the MT gradient (dMT) profile, the large storms' dMT profiles below the 750-hPa level (including 750 hPa) did not pass the significance test. The data points of profiles that passed the significance test (denoted by circles) reveals slight differences between the two: U storms had a smaller dMT value than that of S storms above the 600-hPa level (4.21 km). Hence, temperature fields are unsuitable for distinguishing the storm type.

d. Surface parameters

U and S storms had differences in surface evaporation and ground roughness. Figures 8a and 8b are the box-and-whiskers plots of mean surface evaporation and mean ground roughness. For surface evaporation, the significance values between S and U storms are 0.000 (for small storms) and 0.051 (for large storms). For ground roughness, the significance values between S and U storms are 0.004 (for small storms) and 0.151 (for large storms).

A large negative value for surface evaporation indicated high relative humidity at low levels. The U storms' surface evaporation had a larger negative value than that of S storms. The small storm movement was unsteady when surface roughness was high. Therefore a higher surface evaporation favored the occurrence of U storms, and a higher surface roughness was more conducive to the occurrence of U_S storms.

In the 1100–1400 LST stage (Fig. 3b), the amount of surface evaporation increases with the increase in incoming solar radiation, causing high absolute moisture in the low-level troposphere. The number of convective initiation events begins to increase significantly, indicative of ample unsteadiness. The volume and movement speed of storms was smaller than the average values and lasted until 1400 LST. Thus the occurrence ratio of U storms increased rapidly (further research is required to verify this explanation).

Table 2 shows the number of storms that occurred in different terrain types. As we inferred, the U storms had the highest occurrence ratio (42.01%) over mountains (the highest surface roughness) and the lowest occurrence ratio (31.59%) over ocean (the lowest surface roughness). This also meant that the forecast quality over mountains was much worse than that over ocean and plains.

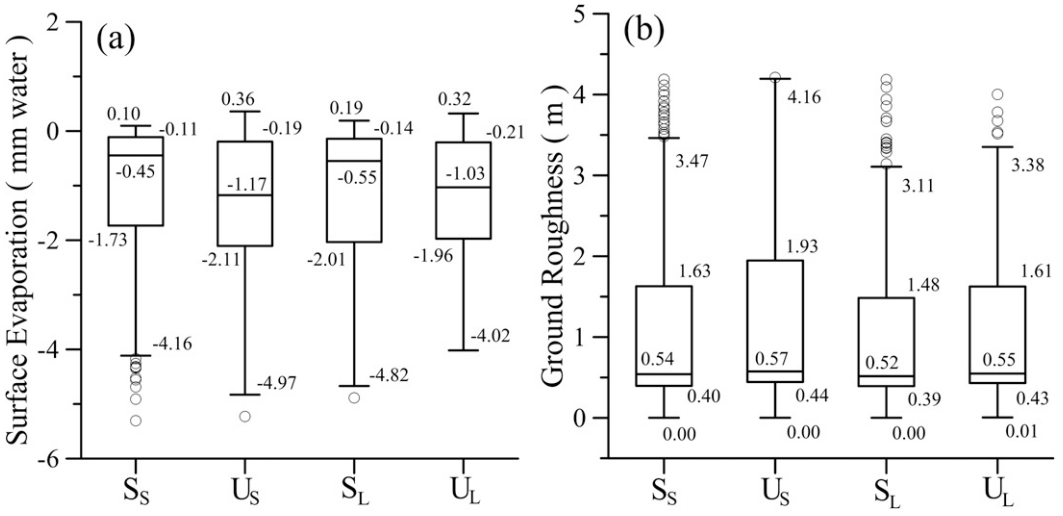

FIG. 8. Box-and-whisker plots of (a) surface evaporation (mm water) and (b) ground roughness (m). The upper and lower ends of the box indicate the quartiles, and the horizontal line inside the box indicates the median value. The whiskers extend from the quartiles to the min and max values. The circles indicate outliers.

We also checked the situation of storms passed differential orographic forcing. Storms that moved from land to water and from water to land were mainly analyzed. The result showed 1) for storms that moved from water to land, the occurrence ratio of S storms and U storms were 46.97% and 34.85%, respectively; and 2) for storms that moved from land to water, the occurrence ratio of S storms and U storms were 47.73% and 29.55%, respectively. As the results in Table 2 show, storms that moved from water to land had a higher chance of being U storms than storms that remained over water, and storms that moved from land to water had a higher chance of being S storms than storms that remained over land.

For S storms, extrapolation methods are normally sufficient. However, auxiliary data (other observation and forecast data) used to guide extrapolation of S storms may cause unexpected errors. Nonetheless, for U storms, auxiliary data are useful for guiding extrapolation. Many factors can affect the steadiness of storm movement. These factors include, but are not limited to, the storm area, thickness, movement speed, vertical velocity, relative wind profile, relative humidity, surface evaporation, and surface characteristics (e.g., orographic forcing and surface roughness).

e. Significance analysis

Although 15% was used as the significance level in previous analysis, it would be useful to know whether the comparisons are significant at the 10% and 5% level. Table 3 listed the ranges or values that did not pass the significance test at the 5% or 10% level but passed the significance test at the 15% level. Because of the following two reasons, some parameters were not shown in Tables 3: 1) the significance level did not impact the test result of speed and storm-relative u and v wind profiles, and 2) the temperature fields are unsuitable for distinguishing the storm type. From Table 3, the significance level had an obviously impact on occurrence ratio, mean area, VV, dVV, RH, and dRH.

5. Conclusions and discussion

According to the MDD (an indicator of the steadiness of storm movement), storms were classified into three types: 1) S storms (MDD $\leq 15°$), 2) U storms (MDD $> 30°$), and 3) T storms ($15° <$ MDD $\leq 30°$). The statistical results of the 6-yr storm data showed that U and S storms had significant differences in geometrical features, dynamical factors, and environmental parameters. The following conditions are more conducive to the emergence of U storms in the Beijing–Tianjin region: 1) a smaller area, 2) a lower thickness (especially below 4 km), 3) a lower movement speed (especially below 5 m s^{-1}), 4) weaker updrafts and the maximum value located in the mid- and upper troposphere, 5) a storm-relative wind profile dominated by the directional shear, 6) lower relative humidity in the mid- and upper

TABLE 2. The number of S, U, and T storms over the ocean, plains, and mountains. The value in parentheses is the occurrence ratio.

	S storm	U storm	T storm
Ocean	868 (44.02%)	623 (31.59%)	481 (24.39%)
Plains	3466 (37.94%)	3366 (36.85%)	2303 (25.21%)
Mountains	1603 (32.03%)	2102 (42.01%)	1299 (25.96%)

TABLE 3. The ranges or values that do not pass the one-sided Wilcoxon-Mann-Whitney rank-sum test at 5% or 10% level but pass the test at the 15% level. In parentheses, S denotes small storms and L denotes large storms.

	5% level	10% level
Occurrence ratio	0000–0200, 0500–0600, 1000–1100, 1800–2000, and 2100–2200 LST	0100–0200, 0500–0600, 1000–1100, and 1800–2000 LST
$\log_{10}$[mean area (km^2)]	1.4–1.5, 2.1–2.2, 2.3–2.4, 2.6–2.7	2.6–2.7
Thickness (km)	7.0–8.0	7.0–8.0
MVV(S) (hPa)	300, 350, 400, 950, and 1000	350 and 400
MVV(L) (hPa)	350, 400, 450, 500, and 1000	—
dMVV(S) (hPa)	450, 500, 550, 600, 800, 825, and 950	—
dMVV(L) (hPa)	400, 500, 550, 600, 650, 750, 850, and 925	550, 600, and 750
MRH(S) (hPa)	1000	1000
MRH(L) (hPa)	400, 600, 875, 900, 925, and 950	600 and 950
dMRH(S) (hPa)	300, 550, 600, 650, 775, 800, 825, 850, and 1000	550, 650, and 850
dMRH(L) (hPa)	350, 400, 875, 900, and 975	975

troposphere, and 7) higher surface evaporation and ground roughness.

For S storms, most extrapolation techniques can give satisfactory results, but for the U storms, the results are poor. Hence, the auxiliary data should be used to guide the extrapolation of U storms. Improving the extrapolation of U storms is an important aspect of improving forecast skill.

In addition, this study focused on the directional steadiness of storms. The effects of different variables on the speed steadiness of storms were not addressed. This should be considered in future work. Also, more comparisons with existing published work (especially in the realm of convection propagation) should be provided in the next step.

Acknowledgments. This research work was supported by the China Special Fund for Meteorological Research in the Public Interest (GYHY201306047) and National Science Funding of China (41275112 and 41005024). Radar data were downloaded from National Meteorological Center of the China Meteorological Agency (NMC/CMA). The authors thank Professor Zuyu Tao and Xiaoyang Liu (Peking University) for their discussion and guidance. The authors thank ECMWF for providing the ERA-Interim data. The authors thank three anonymous reviewers for constructive comments that significantly improved the quality of this paper.

REFERENCES

Browning, K. A., and C. Collier, 1989: Nowcasting of precipitation systems. *Rev. Geophys.,* **27,** 345–370, doi:10.1029/RG027i003p00345.

Coniglio, M. C., S. F. Corfidi, and J. S. Kain, 2011: Environment and early evolution of the 8 May 2009 derecho-producing convective system. *Mon. Wea. Rev.,* **139,** 1083–1102, doi:10.1175/2010MWR3413.1.

——, ——, and ——, 2012: Views on applying RKW theory: An illustration using the 8 May 2009 derecho-producing convective system. *Mon. Wea. Rev.,* **140,** 1023–1043, doi:10.1175/MWR-D-11-00026.1.

Dee, D. P., and Coauthors, 2011: The ERA-Interim reanalysis: Configuration and performance of the data assimilation system. *Quart. J. Roy. Meteor. Soc.,* **137,** 553–597, doi:10.1002/qj.828.

Dixon, M., and G. Wiener, 1993: TITAN: Thunderstorm identification, tracking, analysis and nowcasting—A radar-based methodology. *J. Atmos. Oceanic Technol.,* **10,** 785–797, doi:10.1175/1520-0426(1993)010<0785:TTITAA>2.0.CO;2.

Germann, U., and I. Zawadzki, 2002: Scale-dependence of the predictability of precipitation from continental radar images. Part I: Description of the methodology. *Mon. Wea. Rev.,* **130,** 2859–2873, doi:10.1175/1520-0493(2002)130<2859:SDOTPO>2.0.CO;2.

Golding, B. W., 1998: Nimrod: A system for generating automated very short range forecasts. *Meteor. Appl.,* **5,** 1–16, doi:10.1017/S1350482798000577.

Han, L., S. X. Fu, L. F. Zhao, Y. G. Zheng, H. Q. Wang, and Y. J. Lin, 2009a: 3D convective storm identification, tracking, and forecasting—An enhanced TITAN algorithm. *J. Atmos. Oceanic Technol.,* **26,** 719–732, doi:10.1175/2008JTECHA1084.1.

——, X. D. Yu, Y. G. Zheng, M. X. Chen, H. Q. Wang, and Y. J. Lin, 2009b: Statistic characteristics of severe convective storm during warm-season in the Beijing-Tianjin region and its vicinity. *Chin. Sci. Bull.,* **54,** 2493–2498, doi:10.1007/s11434-009-0085-7.

Jessup, S. M., and S. J. Colucci, 2012: Organization of flash-flood-producing precipitation in the northeast United States. *Wea. Forecasting,* **27,** 345–361, doi:10.1175/WAF-D-11-00026.1.

Kessinger, C., S. Ellis, J. Vanandel, and J. Yee, 2003: The AP clutter mitigation scheme for the WSR-88D. Preprints, *31st Conf. on Radar Meteorology,* Seattle, WA, Amer. Meteor. Soc., 7B.3. [Available online at https://ams.confex.com/ams/pdfpapers/64615.pdf.]

Liang, Q. Q., Y. R. Feng, W. J. Deng, S. Hu, Y. Y. Huang, Q. Zeng, and Z. T. Chen, 2010: A composite approach of radar echo extrapolation based on TREC vectors in combination with model-predicted winds. *Adv. Atmos. Sci.,* **27,** 1119–1130, doi:10.1007/s00376-009-9093-4.

Lin, C., S. Vasić, A. Kilambi, B. Turner, and I. Zawadzki, 2005: Precipitation forecast skill of numerical weather prediction models and radar nowcasts. *Geophys. Res. Lett.,* **32,** L14801, doi:10.1029/2005GL023451.

Liu, L. P., L. L. Wu, and Y. M. Yang, 2007: Development of fuzzy-logical tow-step ground clutter detection algorithm. *Acta Meteor. Sin.,* **65,** 252–260.

Mandapaka, P. V., U. Germann, L. Panziera, and A. Hering, 2012: Can Lagrangian extrapolation of radar fields be used for precipitation nowcasting over complex Alpine orography? *Wea. Forecasting,* **27,** 28–49, doi:10.1175/WAF-D-11-00050.1.

Markowski, P., and Y. Richardson, 2006: On the classification of vertical wind shear as directional shear versus speed shear. *Wea. Forecasting,* **21,** 242–247, doi:10.1175/WAF897.1.

Nisi, L., P. Ambrosetti, and L. Clementi, 2014: Nowcasting severe convection in the Alpine region: The COALITION approach. *Quart. J. Roy. Meteor. Soc.,* **140,** 1684–1699, doi:10.1002/qj.2249.

Orlanski, I., 1975: A rational subdivision of scale for atmospheric processes. *Bull. Amer. Meteor. Soc.,* **56,** 527–530.

Radhakrishna, B., I. Zawadzki, and F. Fabry, 2013: Postprocessing model-predicted rainfall fields in the spectral domain using phase information from radar observations. *J. Atmos. Sci.,* **70,** 1145–1159, doi:10.1175/JAS-D-12-0175.1.

VandenBerg, M. A., M. C. Coniglio, and A. J. Clark, 2014: Comparison of next-day convection-allowing forecasts of storm motion on 1- and 4-km grids. *Wea. Forecasting,* **29,** 878–893, doi:10.1175/WAF-D-14-00011.1.

Wilson, J. W., 2004: Precipitation nowcasting: Past, present and future. *Sixth Int. Symp. on Hydrological Applications of Weather Radar,* Melbourne, VIC, Australia, CAWCR, 8 pp.

——, N. A. Crook, C. K. Mueller, J. Z. Sun, and M. Dixon, 1998: Nowcasting thunderstorms: A status report. *Bull. Amer. Meteor. Soc.,* **79,** 2079–2099, doi:10.1175/1520-0477(1998)079<2079:NTASR>2.0.CO;2.

——, R. F. Ye, M. Chen, and R. D. Roberts, 2010: Nowcasting challenges during the Beijing Olympics: Successes, failures, and implications for future nowcasting systems. *Wea. Forecasting,* **25,** 1691–1714, doi:10.1175/2010WAF2222417.1.

Winterrath, T., and W. Rosenow, 2007: A new module for the tracking of radar-derived precipitation with model-derived winds. *Adv. Geosci.,* **10,** 77–83, doi:10.5194/adgeo-10-77-2007.

Wulfmeyer, V., A. Behrendt, C. Kottmeier, and U. Corsmeier, 2011: The Convective and Orographically-induced Precipitation Study (COPS): The scientific strategy, the field phase, and research highlights. *Quart. J. Roy. Meteor. Soc.,* **137,** 3–30, doi:10.1002/qj.752.

Zahraei, A., K. Hsu, S. Sorooshian, J. J. Gourley, Y. Hong, and A. Behrangi, 2013: Short-term quantitative precipitation forecasting using an object-based approach. *J. Hydrol.,* **483,** 1–15, doi:10.1016/j.jhydrol.2012.09.052.